Commensurate and incommensurate vortex lattice melting in periodic pinning arrays

C. Reichhardt

Center for Nonlinear Studies and Applied Theoretical and Computational Physics Division, Los Alamos National Laboratory, Los Alamos, New Mexico 87545

C. J. Olson

Theoretical and Applied Physics Divisions, Los Alamos National Laboratory, Los Alamos, New Mexico 87545

R. T. Scalettar and G. T. Zimányi

Department of Physics, University of California—Davis, Davis, California 95616

We examine the melting of commensurate and incommensurate vortex lattices interacting with square pinning arrays through the use of numerical simulations. For weak pinning strength in the commensurate case we observe an order-order transition from a commensurate square vortex lattice to a triangular floating solid phase as a function of temperature. This floating solid phase melts into a liquid at still higher temperature. For strong pinning there is only a single transition from the square pinned lattice to the liquid state. For strong pinning in the incommensurate case, we observe a multistage melting in which the interstitial vortices become mobile first, followed by the melting of the entire lattice, consistent with recent imaging experiments. The initial motion of vortices in the incommensurate phase occurs by an exchange process of interstitial vortices with vortices located at the pinning sites. We have also examined the vortex melting behavior for higher matching fields and find that a coexistence of a commensurate pinned vortex solid with an interstitial vortex liquid occurs while at higher temperatures the entire vortex lattice melts. For triangular arrays at incommensurate fields higher than the first matching field we observe that the initial vortex motion can occur through a correlated ring excitation where a number of vortices can rotate around a pinned vortex. We also discuss the relevance of our results to recent experiments of colloidal particles interacting with periodic trap arrays.

I. INTRODUCTION

Vortices interacting with periodic pinning arrays have attracted growing interest with the advances of nanolithographic techniques in which the size and shape of individual pinning sites, as well as the geometry of the pinning array, can be carefully controlled. These pinning arrays can be composed of 1D periodic modulations,[1] microholes[2–8] or magnetic dots[9–11] in which the holes or dots have a diameter d significantly less than the dot spacing a. The holes and dots suppress the order parameter, allowing the flux lines in the mixed state to lower their energy, and thereby pinning the vortices. Strong commensurability effects in these systems are observed at the matching fields, when the number of particles equals an integer multiple of the number of divots.[2–4,9,12] Transport measurements near T_c above the first matching field indicate that some of the vortices are only weakly pinned in the interstitial regions. These vortices become mobile at a lower applied current than the vortices at the pinning sites.[6] Direct evidence for commensurate states and interstitial vortices has been obtained using Lorentz force microscopy[5] and scanning Hall probe microscopy.[7,8] Magnetization measurements by Baert *et al.*[3] interpreted the loss of pinning above the first matching field near T_c as due to a coexistence of an interstitial vortex liquid with a pinned vortex solid at the pinning sites.

In addition to the technological applications of superconductors which require strong pinning, vortices interacting with periodic pinning arrays are also an ideal realization of an elastic lattice interacting with a periodic substrate which can be generalized to a wide variety of condensed matter systems including atoms adsorbed on a surface,[13] colloidal crystals interacting with interfering laser beams,[14] and vortices in Josephson-junction arrays.[15,16] A very similar system to vortices in periodic arrays that has recently been experimentally realized is colloidal particles interacting with optical trap arrays.[17–20] Recent experiments in these systems for colloids interacting with a square array observed an interesting transition from a commensurate square colloidal crystal to a triangular colloidal crystal for increasing colloidal densities when the colloidal interactions began to dominate over the substrate.[19]

Although studies of the effects of temperature have been conducted on the dynamics of vortices interacting with periodic pinning arrays,[21] the static melting has not been investigated. Here one could expect that vortex lattice melting behavior may be significantly different at commensurate vs incommensurate fields. Melting of vortices in wire networks has been studied[15] for systems for filling fractions far less than one with Monte Carlo simulations. The Monte Carlo simulations of vortices in wire networks at low filling factors by Franz and Teitel[15] have shown a transition from a pinned solid to a floating solid phase, both of which have the same symmetry as the underlying pinning lattice. For higher temperatures this floating solid phase was found to melt into a liquid. In the wire network case there are no interstitial regions, and at the matching field the floating solid phase is absent.[15] The wire network system has several differences

from vortices in periodic arrays in that in the former the vortices can be considered to move in an egg-carton potential. For vortices in periodic arrays the vortices would move in a muffin-tin substrate in which there are flat potential regions between the minima. In this system at low temperatures at commensurate matching, particles in the overlying lattice will sit in the divots or energy minima, while at the incommensurate matching, some particles will sit in the *interstitial* regions between the divots.[5,6,12] Even at the matching field it can be possible for vortices to move into the interstitial regions when the vortex-vortex interactions become dominant or thermal fluctuations are strong enough.

Another difference between vortices in wire networks compared to vortices in periodic pinning arrays appears for fields greater than the first matching field. The additional vortices in the imaging experiments by Harada *et al.*[5] and simulations by Reichhardt *et al.*[12] indicate that in periodic pinning arrays a wide variety of interstitial vortex crystals can be stabilized at different matching fields.

The vortices located in the interstitial regions can have significantly different static, dynamic and thermal properties than the commensurate particles, and the coupling between the two different species can give rise to interesting behavior. Recent imaging experiments by Grigorenko *et al.*[7] using high resolution scanning Hall probe microscopy near the matching field B_ϕ indicate that, for fields slightly below and above the first matching field, over time the vacancies and interstitials appear to show site to site hopping. The nature of the hopping dynamics is however not known, such as whether the interstitial vortices jump from one interstitial site to another or if the interstitials undergo an exchange process with the vortices at the pinning sites. These experiments were done for square arrays and it is not known how the vortex hopping might occur in different geometries such as triangular pinning arrays.

The melting of interstitial vortices which coexist with strongly pinned vortices has also been proposed by Radzihovsky[22] for vortices interacting with randomly placed columnar defects where there are more vortices than pinning sites.

In this work we report the study of two-dimensional melting of vortices interacting with a square muffin tin pinning potential with the use of molecular dynamics simulations. For the commensurate case at low substrate strengths we observe a different order-order transition from a square pinned vortex lattice with long-range order to a triangular ordered floating solid phase with quasi-long-range order. Our simulations also allow us to examine the vortex dynamics at the transition into the floating solid where the vortices show a collective 1D avalanche motion along the pinning rows. For increased substrate strength the floating solid phase is lost and the pinned solid melts directly to a liquid. In the incommensurate case for vortex densities slightly above the first matching field for strong substrates we observe a multistage melting in which the initial vortex motion occurs by an exchange process of interstitial and pinned vortices.

We have also examined the effects of temperature for higher matching and nonmatching fields greater than one. At the higher matching fields we find that the vortices form a solid at low temperatures. For higher temperatures we observe a coexistence of an interstitial vortex liquid with a pinned vortex solid in agreement with the experiments of Baert *et al.* At high incommensurate fields the extra vortices or vacancies in the interstitial vortex liquid become mobile. We observe the same general behaviors for triangular pinning arrays; however, at the incommensurate fields the motion of extra vortices or vacancies can occur by novel collective ring excitations where a group of vortices rotate around a vortex in a pinning site. These excitations occur when an incommensurate number of vortices cage a vortex located at a pinning site.

Our system should not only be of relevance for vortices and colloids interacting with periodic substrates but also for the square to hexatic vortex transitions observed in certain superconductors,[23–26] where little is known about the dynamics at the transitions.

II. SIMULATION

We model a 2D system with periodic boundary conditions in x and y with N_v vortices interacting with a square array of N_p pinning sites. We use a Langevin simulation for vortices at finite temperature using the model of Brass and Jensen.[27,28] We consider the vortex motion to be overdamped and integrate the following equation of motion:

$$\mathbf{f}_i = \eta\mathbf{v}_i = \mathbf{f}_i^{vv} + \mathbf{f}_i^{vp} + \mathbf{f}_i^T. \qquad (1)$$

Here $\mathbf{f}_i$ is the total force acting on vortex i and η is the damping coefficient. The repulsive interaction of vortex i with the other vortices is $\mathbf{f}_i^{vv} = \Sigma_{j=1}^{N_v} f_0 K_1(|\mathbf{r}_i-\mathbf{r}_j|/\lambda)\hat{\mathbf{r}}_{ij}$. Here, λ is the penetration depth and $K_1(r/\lambda)$ is a modified Bessel function which falls off exponentially for $r>\lambda$, allowing us to place a cutoff in the interactions at $r=6\lambda$ for computational efficiency. The pinning is modeled as N_p parabolic traps with $\mathbf{f}_i^{vp} = -\Sigma_{k=1}^{N_p}(f_p/r_p)(|\mathbf{r}_i-\mathbf{r}_k^{(p)}|)\Theta(r_p -|\mathbf{r}_i-\mathbf{r}_k^{(p)}|)\hat{\mathbf{r}}_{ik}^{(p)}$. Here, Θ is the Heaviside step function, r_p is the range of the pinning potential, f_p is the maximum pinning force of the wells, $\hat{\mathbf{r}}_{ij}=(\mathbf{r}_i-\mathbf{r}_j)/|\mathbf{r}_i-\mathbf{r}_j|$ and $\hat{\mathbf{r}}_{ik}^{(p)} = (\mathbf{r}_i-\mathbf{r}_k^{(p)})/|\mathbf{r}_i-\mathbf{r}_k^{(p)}|$. The thermal force has the properties $\langle f_i^T(t)\rangle=0$ and $\langle f_i^T(t)f_j^T(t')\rangle=2\eta k_B T \delta_{ij}\delta(t-t')$. In this work we set $\eta=k_B=1$. All lengths, fields and forces are given in units of λ, Φ_0/λ^2 and f_0, respectively. For most of the results shown here the density of vortices is $0.25\Phi_0/\lambda^2$. The initial ground state of the system is found using simulated annealing. We then slowly increase T and analyze the coordination number, P_n (from the Voronoi or Wigner Seitz cell construction), and the structure factor,

$$S(\mathbf{k})=(1/L^2)\sum_{i,j} e^{i\mathbf{k}\cdot[\mathbf{r}_i-\mathbf{r}_j]},$$

where L is the system size length.

Another measure we employ to characterize the thermally induced transition is the sum of the displacements of the vortices from their initial positions at $T=0$ to their positions at a higher T:
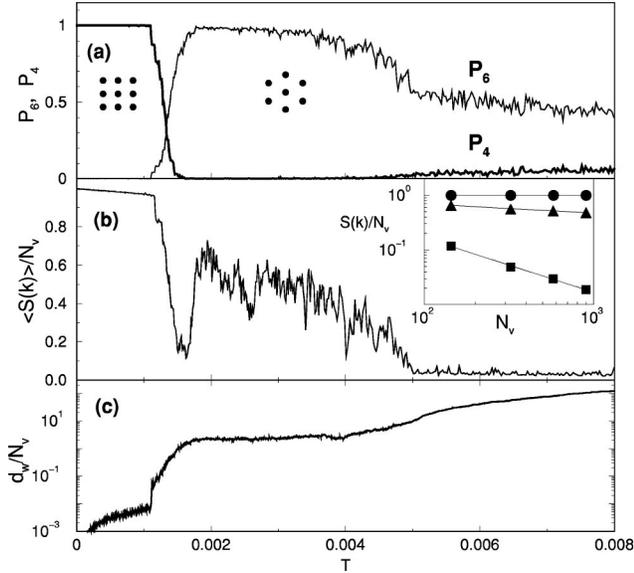
FIG. 1. (a) The fraction of fourfold P_4 (thick line) and sixfold P_6 coordinated (thin line) vortices versus T. (b) The average power of the secondary peaks, $\langle S(\mathbf{k})\rangle/N_v$ versus T. The position of the peaks shifts from fourfold to sixfold near $T=0.001$. The peaks are lost at $T=0.005$. The inset of (b) shows the scaling of the secondary peaks for different system sizes where $N_v \sim L^2$. For the pinned phase (circles), $T=0.0005$ and $S(k) \sim L^0$; for the triangular lattice (triangles), $T=0.003$ and $S(k) \sim L^{-0.33}$; and for the liquid phase (squares), $T=0.007$ and $S(k) \sim L^{-1.98}$. (c) The displacements $d_w/N_v = \langle |\mathbf{r}(T) - \mathbf{r}(0)|^2\rangle$ of the vortices versus T.

$$d_w(T) = \sum_{i=1}^{N_v} |\mathbf{r}_i(T) - \mathbf{r}_i(0)|^2.$$

If the vortex lattice configuration is the same as the initial state than $d_w=0$. If a portion of the vortices move but then become frozen again d_w will jump up. If the vortex lattice becomes molten d_w will increase to a saturation value of $L/2$.

To visualize vortex motion we plot the trajectories that the vortices follow for a period of time. To examine the dynamic response in the phases we can add a driving term $\mathbf{f}_i^d$ representing a Lorentz force from an applied current to Eq. (1) and sum over the net vortex velocities $V_x = \Sigma_{j=1}^{N_v} \mathbf{v}_i \cdot \hat{\mathbf{x}}$. To analyze finite size scaling in $S(\mathbf{k})$ we conduct simulations with the same vortex and pin densities for system sizes with a length L for systems ranging from $L=24\lambda$ to $L=60\lambda$ with $N_v=144$ to $N_v=900$.

III. COMMENSURATE MELTING

In Fig. 1 we present the evolution of the coordination numbers P_6 and P_4, the average power of the secondary peaks in the structure factor $\langle S(\mathbf{k})\rangle$, and the vortex displacements d_w for increasing T for a system at the matching field with $L=48\lambda$. Here $f_p=0.03f_0$, $r_p=0.17\lambda$, and $a=2.0\lambda$. For $0<T<0.0012$ the pinned vortex lattice has the same square symmetry as the pinning lattice, as indicated by $P_4 \approx 1.0$. The initial increase in d_w for $T<0.0012$ is due to the vortices moving randomly within pinning sites but remaining

confined to a distance r_p. Near $T=0.0012$ there is a structural transition in the vortex lattice from square lattice to triangular, indicated by the sudden drop in P_4 to ~ 0 and the large increase in P_6 to 0.98. In Fig. 1(b) we plot the average $\langle S(\mathbf{k})\rangle$ of the appropriate secondary peaks in $S(\mathbf{k})$. For $T < 0.0012$ we observe only four secondary peaks in $S(\mathbf{k})$ as indicated in the left inset in Fig. 1(a). At the square-triangular transition there is initially a large drop in $\langle S(\mathbf{k})\rangle$ from 0.95 to 0.2 and then a recovery to 0.55. The position of the secondary peaks shifts at the transition from fourfold to sixfold order. During the transition a mixture of *both* four and sixfold peaks appear, reducing the overall power at each peak. In the triangular phase there is almost no power for the fourfold order. The square to triangular transition can also be observed as a jump in d_w [Fig. 1(c)], coinciding with the drops in P_4 and $\langle S(\mathbf{k})\rangle$, which is due to the shifting of the vortex positions during the transition. In the triangular lattice phase, d_w remains roughly constant, indicating that diffusion is not occurring and that the vortex lattice is still a solid. Near $T=0.0049$ the triangular vortex lattice melts into a liquid, indicated by the increase in d_w as well as the drops in $\langle S(\mathbf{k})\rangle$ and P_6. We note that P_6 will not drop to zero for a liquid state since even for random particle distributions a portion of the vortices will always have sixfold coordination numbers. We have also conducted simulations where we cool down in temperature starting at $T=0.008$. In this case we do not observe any hysteresis in the liquid to triangular phase; however, hysteresis is present in the triangular to square transition, suggesting that the transition is first order in nature. We have also examined the response of the phase to an applied drive and find that only the square pinned phase has a finite critical depinning force.

The finite size scaling behavior of the structure factor

$$S(\mathbf{k})/L^2 \sim L^{-\theta},$$

which is described more fully in Ref. 15 gives us further information about the nature of the phases. For long range order, $\theta=0$, for floating solids or hexatic phases $0<\theta<2.0$, and for the liquid phase $\theta=2.0$. For different system sizes we average the power of the secondary peaks in $\langle S(\mathbf{k})\rangle$ for 150 frames. In the inset of Fig. 1(b) we plot $\langle S(\mathbf{k})\rangle/L^2$ (where $N_v \sim L^2$) versus N_v for the three different phases. In the commensurate phase ($T=0.0005$) we find $\theta \approx 0.0$ corresponding to the pinned lattice. For $T=0.003$, in the triangular phase, $\theta=0.33\pm0.04$ which is consistent with a floating solid phase. In the floating solid phase we find a small variation of θ with T which we will address elsewhere. In the liquid phase ($T=0.007$) we find $\theta=1.98\pm0.04$.

A. Dynamics of the order-order transition

In order to gain insight into the dynamics of the square to triangular transition, in Fig. 2 we show the real space images as well as the individual vortex trajectories in the pinned solid, the pinned-solid to floating solid transition, and the liquid phase for the system in Fig. 1. In the pinned solid phase shown in Fig. 2(a) ($T=0.0005$) we find a square vortex lattice with little or no detectable vortex motion. Figure 2(b) ($T=0.00135$) shows the *dynamics* at the beginning of
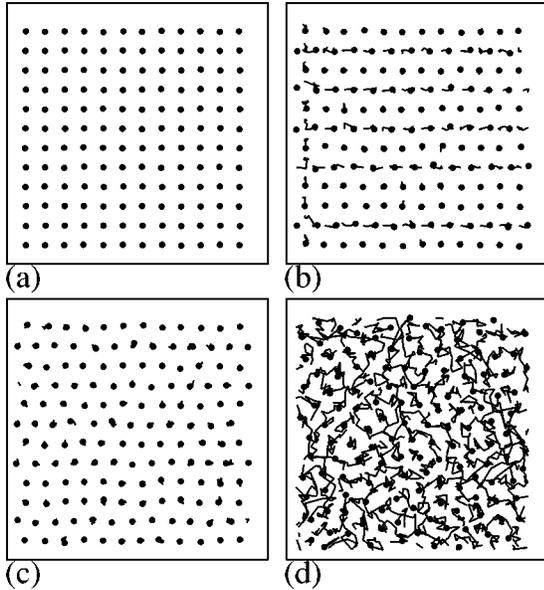
FIG. 2. The vortex positions and trajectories for a $24\lambda \times 24\lambda$ section of a $48\lambda \times 48\lambda$ system for (a) the pinned solid ($T = 0.0005$), (b) the beginning of the pinned solid to floating solid transition ($T = 0.00135$), (c) the floating solid phase ($T = 0.0015$), and (d) the liquid phase ($T = 0.0065$). In (b) alternate rows of vortices shift positions. For slightly higher temperatures the other vortices also shift in position. This shifting is reflected in the jump in d_w at $T = 0.0012$ in Fig. 1(c).

the pinned to floating solid transition. Here alternate rows of vortices move in a sudden 1D avalanche where the vortices in one row move in a collective manner while the other rows remain static. All the vortices in a given row shift together as the vortices jump out of the pinning sites and move to the interstitial regions. The motionless rows shown in Fig. 2(b) also begin to move at a slightly later time. This shifting of the vortex positions produces the jump in d_w at $T = 0.0012$ seen in Fig. 1(c) at the square to floating solid transition. In Fig. 2(c) ($T = 0.0015$), in the floating solid phase, the vortex lattice has triangular order and shows increased thermal wandering around the equilibrium positions as can be seen in the vortex trajectories. This increased thermal wandering also smears the secondary peaks in $S(\mathbf{k})$, reducing the maximum value to 0.55, as in Fig. 1(b). In Fig. 2(d) ($T = 0.0065$), in the molten state the vortices are disordered and diffuse in a random manner corresponding to the large value of d_w in Fig. 1(c).

B. Phase diagram for the commensurate case

By conducting a series of simulations with different substrate strengths and using the criteria from Fig. 1 to determine the onset of the different phases, we construct the phase diagram in Fig. 3. The range of temperatures over which the commensurate solid appears increases linearly for increasing f_p. The floating solid phase only appears for $f_p < 0.125f_0$. The line separating the floating solid to liquid phase is roughly constant with temperature for lower substrate strengths at a value that corresponds to roughly the zero pin-
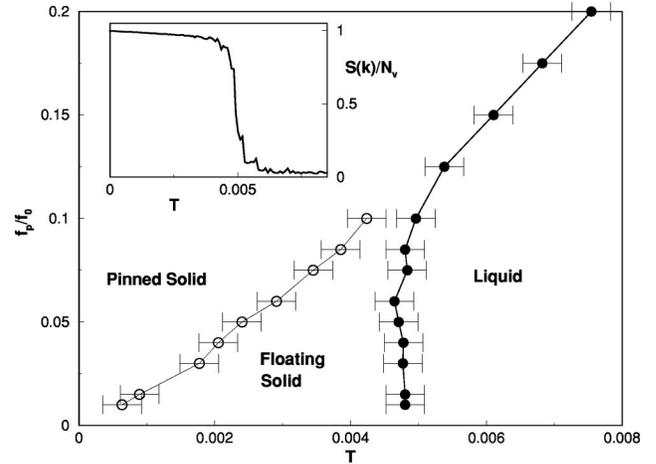

FIG. 3. The phase diagram of f_p versus T. The open circles represent the pinned solid to floating solid transition. The filled circles represent the transition into the liquid phase. The inset shows the behavior of $\langle S(\mathbf{k}) \rangle / N_v$ versus T for $f_p = 0.125f_0$ where the pinned solid melts directly to a liquid.

ning melting temperature, $T_m = 0.0048$ (as also obtained with the diffusion and structure factor measurements). All three phase boundaries can be understood from simple considerations. The floating solid to liquid line is independent of f_p because it is determined by the vortex-vortex interactions and not the pinning force. For $f_p \geq 0.125f_0$ the commensurate solid melts directly into a liquid and $\langle S(\mathbf{k}) \rangle$ has the behavior shown in the inset of Fig. 3. The melting transition is seen to shift to *higher* temperatures with increasing pinning strength, as the melting occurs when thermal fluctuations are able to overcome the increasing pinning strength. Finally the commensurate-to-floating solid follows $f_p \sim T$ with the low f_p being washed out before the vortex-vortex interactions are washed out. The nature of the floating solid to liquid transition, such as whether a dislocation-mediated melting transition occurs,[13] is beyond the scope of this work.

To further compare our results with those of vortices in wire networks,[15] in which the floating solid phase with the same symmetry as the pinned phase is observed as a function of commensurability, in our case the pinned to floating solid transition is seen as a function of substrate strength. Further, we observe a square to triangular transition due to the fact that a portion of the vortices shift into pin free regions, which is not possible in wire networks.

We note that in our simulation we imposed nearly square boundary conditions which can create defects or stress in the triangular lattice. We do not find any defects in our triangular lattice and our finite size scaling is consistent with that in Ref. 15. It is also possible that the square pinned solid phase may be enhanced for a higher temperature range by the square boundary conditions; however, the general trends of the phase diagram should still hold.

IV. INCOMMENSURATE MELTING NEAR THE FIRST MATCHING FIELD

We now consider the vortex behavior above the first matching field when there are more vortices than pins. We
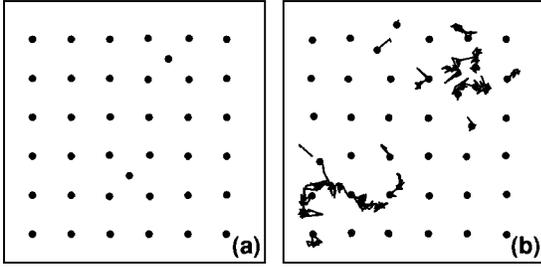
FIG. 4. (a) A snapshot of a $10\lambda \times 10\lambda$ region of the sample with $B/B_\phi = 1.06$. The vortex positions and trajectories for $T = 0.0005$ show that some vortices are pinned at interstitial positions. (b) At $T = 0.0036$ the motion of incommensurations can be seen while the background lattice remains pinned. The vortex trajectories in (b) show that vortex motion occurs by the interstitial vortices pushing other vortices off the pinning sites which in turn move into interstitial regions and repeat the process.

find that for large substrate strengths, $f_p > 0.25 f_0$, a commensurate sublattice forms, with the additional vortices sitting in the interstitial regions. In Fig. 4 we show the melting behavior for a system with $N_v = 1.063 N_p$ and $f_p = 0.6 f_0$. In the imaging experiments of Grigorenko *et al.*,[7] the interstitial motion was observed for a field of $B/B_\phi = 1.04$. Here, for $T < 0.0016$ both the commensurate vortices and the interstitial vortices remain pinned as seen in Fig. 4(a). At these low temperatures, the interstitial vortices are pinned by the potential cage created by vortices at the pinning sites. At $T > 0.0016$ vortex diffusion begins to occur as indicated by the increase in d_w in Fig. 5(b). This is due to the onset of motion of the incommensurations as seen in the vortex trajectories in Fig. 4(b). The motion is *not* restricted to interstitial vortices. Instead, interstitial and pinned vortices *exchange places*, and over a period of time *all* the vortices take part in the motion. The exchange process can be understood by considering that the interstitial vortex will produce a force f_{in} on the nearby commensurate vortices which effectively reduces the pinning force to $|f_p| - |f_{in}|$. Since the melting transition is a function
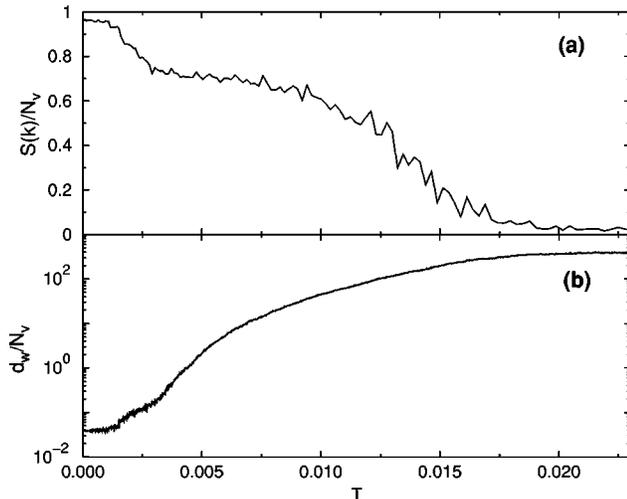

FIG. 5. The behavior of $\langle S(\mathbf{k}) \rangle / N_v$ and d_w / N_v versus T for a system with $f_p = 0.6 f_0$ and $N_v = 1.063 N_p$. Motion in the vortex lattice starts at $T = 0.0016$ as indicated in the increase in d (b).

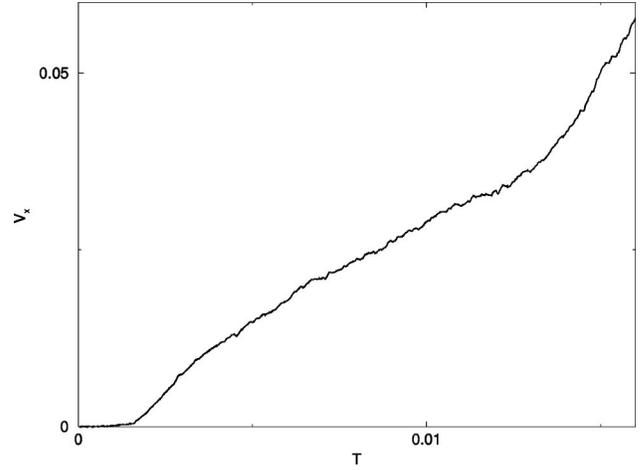

FIG. 6. The behavior of V_x as a function of T.

of the pinning force the melting temperature will be reduced.

In Fig. 5(a) the onset of the incommensuration motion is also marked by a drop in $\langle S(\mathbf{k}) \rangle$ from 0.96 to approximately 0.7. In contrast to the sharp drop in $\langle S(\mathbf{k}) \rangle$ seen in the commensurate case, here $\langle S(\mathbf{k}) \rangle$ still retains strong fourfold order due to the presence of the background lattice of pinned vortices as seen in Fig. 4(b). For higher temperatures $\langle S(\mathbf{k}) \rangle$ gradually decreases with most order being lost for $T > 0.0175$, corresponding to the melting temperature for the commensurate case with the same substrate strength. For simulations where we cool down from $T > 0.0175$ we do not observe any hysteresis. We have also conducted simulations in which we apply a constant drive of $f_d = 0.012$, gradually increase T and measure the average vortex velocity $\langle V_x \rangle$. For $T < 0.0016$, in the pinned interstitial phase $\langle V_x \rangle = 0$. At the interstitial transition there is a jump in $\langle V_x \rangle$ indicating the onset of vortex motion. Finally at the overall vortex melting transition, $\langle V_x \rangle$ jumps to a value corresponding to the entire lattice flowing. This behavior in V_x as a function of T is shown in Fig. 6.

V. MELTING FOR HIGHER COMMENSURATE AND INCOMMENSURATE FIELDS

A. Commensurate melting

We have also investigated the melting in square and triangular pinning arrays for the higher matching fields $B/B_\phi = 2, 3, 4, 5$, and 8. At these fields ordered vortex crystals are formed.[5,12] In Fig. 7 we show the vortex positions and trajectories for the square pinning array with $B/B_\phi = 4.0$ for increasing temperatures. For $T < 0.004$ the vortex lattice is ordered as seen in experiments and simulations. For $T > 0.004$ [Fig. 7(b)] the interstitial vortex lattice melts; however, the vortices at the pinning sites remain immobile so that a coexistence of a solid and a liquid phase occurs. The interstitial vortices are constrained to move in a square grid and there is a region around the pinning sites which the interstitial vortices do not enter due to the repulsion of the vortices located at the pinning sites. Under an applied drive the depinning force is finite for low temperatures but goes to zero
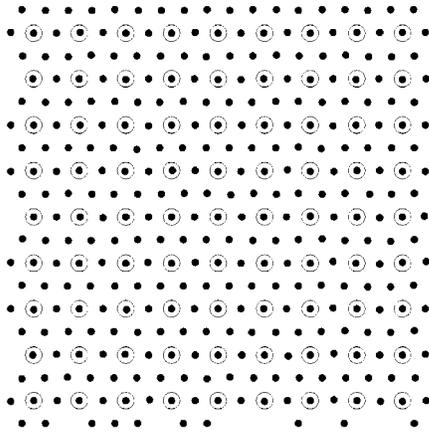
(a)
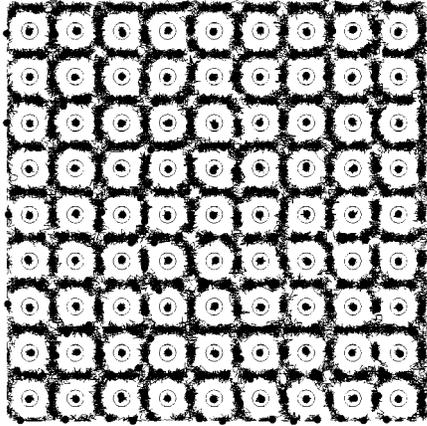
(b)
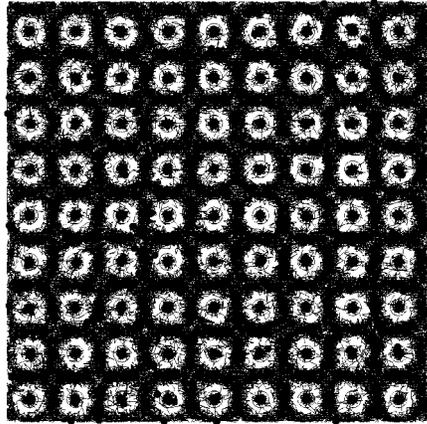
(c)

FIG. 7. (a) The vortex positions (black circles) and pinning sites (open circles) for $B/B_\phi=4.0$ for a system with a square pinning array at $T=0.001$. Here the vortex system is in a crystalline state. (b) For $T=0.004$ the vortex trajectories show that the interstitial vortices are in a liquid state while the vortices at the pinning sites remain immobile. (c) At $T=0.01$ all the vortices are mobile.

at the onset of the interstitial vortex liquid transition. This result is in agreement with the interpretations of the experiments by Baert *et al.* in which the pinning force goes to zero near T_c when interstitial vortices are present, but is still finite
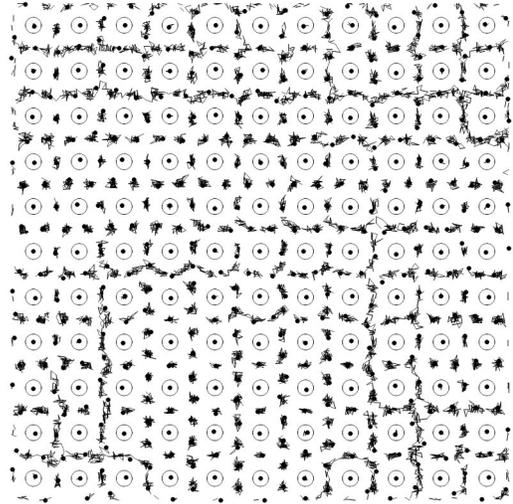

FIG. 8. The vortex positions (black circles) and pinning sites (open circles) for a system with the same pinning parameters as in Fig. 6 for $B/B_\phi=4.1$. Here $T=0.001$ and the vortex trajectories show a portion of the interstitial vortices are mobile.

for fields at which vortices are only located at the pinning sites. For increased T, as in Fig. 7(c), the vortices at the pinning sites become depinned as well and the entire lattice is in the molten state. The general behavior of the melting from Fig. 7 is also seen at the other matching fields we have investigated with transitions from the solid, to solid-liquid coexistence, to the liquid state.

B. Incommensurate melting

In Fig. 8 we show the melting behavior for the incommensurate field $B/B_\phi=4.1$. Here the onset of vortex diffusion occurs for a much lower temperature than for $B/B_\phi=4.0$. The vortex motion occurs at defect sites where additional interstitial vortices are present in the ordered $B/B_\phi=4.0$ interstitial vortex crystal. These extra interstitial vortices are less strongly pinned than the other interstitial vortices. The vortex motion can occur by the continuous motion of a single vortex over a certain distance, or by a pulse-like motion in which a series of individual vortices move by one lattice constant as the pulse moves through. If the trajectories are drawn for a longer time period the interstitial vortex diffusion can be seen to occur through the entire lattice. As the temperature is increased the vortices at the pinning sites will become depinned.

C. Collective ring excitations for incommensurate fields with triangular pinning

We have found that the melting behavior for square and triangular pinning arrays is similar at the matching fields; however, at the incommensurate fields we observe clear differences between the two pinning geometries. In Fig. 9 we show the melting behavior for a system with triangular pinning for $B/B_\phi=3.08$. At low temperatures the system is frozen but as T is increased motion begins to occur in the form of ring excitations. Here a portion of the vortices rotate
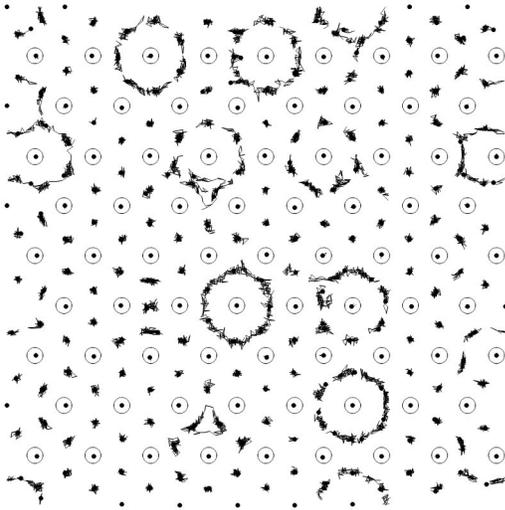
FIG. 9. The vortex positions (black circles) and pinning sites (open circles) for a system with the same parameters as in Fig. 6 with a triangular pinning array with $B/B_\phi = 3.08$ and $T = 0.001$. Here the vortex motion can be seen to occur in a ring excitation where vortices can rotate around pinned vortices. The ring excitations occur where there are seven vortices around a pinned vortex. A second type of excitation can be seen in the trianglular trajectories where three vortices can rotate.

around a vortex at a pinning site; however, no net diffusion of interstitial vortices is occurring. For $B/B_\phi = 3.0$ each vortex at a pinning site is surrounded by six interstitial vortices. For fields above or below $B/B_\phi = 3.0$ a portion of the pinned vortices will be surrounded by 5 or 7 vortices, and it is at these sites where the ring excitations occur. Due to the symmetry of the pinning array the vortices at the pinning sites create a potential around each pinning site which has six minima, so that at $B/B_\phi = 3.0$ the vortex configuration is particularly stable. When there are seven or five vortices around a pinning site, they are incommensurate with the six mimima, and therefore the thermal kicks can cause the interstitial vortices to slowly rotate.

As the applied field is moved further away from the matching field, the number of incommensurations increases and the number of ring excitations increases as well. Such ring excitations are observed in triangular pinning arrays for most incommensurate fields but with different numbers of vortices forming the ring. As the temperature increases, the initial diffusion of the vortices occurs via a hopping mechanism in which the extra vortex in the rotating ring hops out of the ring and starts the rotation of a different ring. The rate of this hopping increases with the temperature.

VI. SUMMARY

In summary, we have investigated the melting of vortex lattices interacting with periodic pinning arrays for both the commensurate and incommensurate case. For the first matching field with weak substrates we have observed a transition in the vortex lattice from a square commensurate solid to a triangular floating solid which melts into a liquid at higher temperatures. This transition occurs by 1D collective motion

of vortices shifting from the pinning sites into the interstitial regions. For strong substrates the floating solid phase is lost and the vortex lattice melts directly into a liquid. For fields slightly above the first matching field for strong disorder we observe a multistage melting where the interstitial vortices are highly mobile consistent with recent imaging experiments. The motion of the interstitial vortices occurs by the exchange of interstitial with pinned vortices rather than with the interstitials hopping from one interstitial site to another. As the temperature increases more vortices become mobile.

We have also examined the melting behavior for matching fields greater than one. At low temperature the interstitial vortices form a crystalline state. At higher temperatures we observe a coexistence of an interstitial vortex liquid with a commensurate pinned vortex lattice. The interstitial vortices can diffuse in the regions between the pinned vortices. We also observe a depletion zone around the pinned vortices which interstitial vortices do not enter due to the repulsion from the pinned vortex. At higher temperatures the entire vortex lattice melts. At higher incommensurate fields the additional defects (extra interstitials or vacancies) in the interstitial vortex crystal become mobile and diffuse in the interstitial regions. With triangular pinning arrays at incommensurate fields the initial vortex motion occurs through a different collective ring excitation where interstitial vortices can rotate around a pinned vortex. These rotations occur when an incommensurate number of interstitial vortices surround a pinned vortex.

We briefly discuss some experimental systems in which these effects could be observed. For vortex lattices in periodic pinning arrays, vortex lattice melting is most relevant to high-T_c superconductors. Our results are only for a 2D system whereas 3D effects can be relevant to melting. Our model would thus best describe high-temperature superconductors with periodic columnar defects where the vortices would have line-like behavior. However, several of the results here should still be relevant for low temperature superconductors. For the low temperature superconductors melting would only occur very near T_c. For strong pinning such as arrays of holes, a floating solid phase at the first matching field would not be observable and the system should go directly from the pinned solid to the normal phase with a very small region of a disordered vortex lattice. For weak pinning such as small magnetic dots or weak defect arrays the pinned solid to floating solid transition should occur well below T_c and should be observable for the low temperature superconductors. For a low temperature superconductor the phase diagram in Fig. 3 would be modified, with the floating solid to liquid transition replaced by the floating solid to normal transition, although again a small vortex liquid state may occur just below T_c. Also the pinned solid to vortex liquid transition would remain flat rather than increasing with f_p. The solid to floating solid transition could be imaged with scanning Hall probe measurements, neutron scattering, or Lorentz microscopy. In addition transport measurements would also be able to reveal the loss of pinning at the transition.

The vortex behavior at the incommensurate fields should also be visible in the low-temperature superconductors. The recent imaging experiments of Grigorenko *et al.*[7] have al-

ready found evidence for the motion of the highly mobile interstitial vortices in these types of systems. These same imaging techniques should be able to image the pinned vortex lattice coexisting with the interstitial vortex liquid. In triangular pinning arrays collective ring excitations would appear as a smeared ring around pinning sites with the Hall probe arrays and the dynamics could be directly imaged with Lorentz microscopy.

Our work is also directly relevant to colloidal particles interacting with periodic pinning. A particularly promising realization of this system is optical trap arrays in which the pinning strength can be easily tuned. In such a system our phase diagram can be directly tested. Recent experiments have already seen evidence for a square to triangular transition as the colloid density is increased.[19] In addition the dynamics of the interstitial colloids can be directly imaged with video microscopy to determine if the interstitials hop directly from one interstitial site to another, or if they move through an exchange process with a pinned colloid. In addition it should also be possible to observe the melting behavior for higher matching colloidal densities and the collective ring excitations for colloids interacting with triangular optical trap arrays.

[1] O. Daldini, P. Martinoli, J.L. Olson, and G. Gerner, Phys. Rev. Lett. **32**, 218 (1974).

[2] A.T. Fiory, A.F. Hebard, and S. Somekh, Appl. Phys. Lett. **32**, 73 (1978).

[3] M. Baert, V.V. Metlushko, R. Jonckheere, V.V. Moschalkov, and Y. Bruynseraede, Phys. Rev. Lett. **74**, 3269 (1995).

[4] V.V. Moshchalkov, M. Baert, V.V. Metlushko, E. Rosseel, M.J. Van Bael, K. Temst, R. Jonckheere, and Y. Bruynseraede, Phys. Rev. B **54**, 7385 (1996); J.Y. Lin, M. Gurvitch, S.K. Tolpygo, A. Bourdillon, S.Y. Hou, and J.M. Phillips, *ibid.* **54**, R12 717 (1996); A. Bezryadin, Yu.N. Ovchinnikov, and B. Pannetier, *ibid.* **53**, 8553 (1996); A. Castellanos, R. Wordenweber, G. Ockenfuss, A.v.d. Hart, and K. Keck, Appl. Phys. Lett. **71**, 962 (1997); V.V. Moshchalkov, M. Baert, V.V. Metlushko, E. Rosseel, M.J. Van Bael, K. Temst, Y. Bruynseraede, and R. Jonckheere, Phys. Rev. B **57**, 3615 (1998); V. Metlushko, U. Welp, G.W. Crabtree, Z. Zhang, S.R.J. Brueck, B. Watkins, L.E. DeLong, B. Ilic, K. Chung, and P.J. Hesketh, *ibid.* **59**, 603 (1999); V. Metlushko, U. Welp, G.W. Crabtree, R. Osgood, S.D. Bader, L.E. DeLong, Z. Zhang, S.R.J. Brueck, B. Ilic, K. Chung, and P.J. Hesketh, *ibid.* **60**, R12 585 (1999).

[5] K. Harada, O. Kamimura, H. Kasai, F. Matsuda, A. Tonomura, and V.V. Moschalkov, Science **271**, 1393 (1996).

[6] E. Rossel, M. Van Bael, M. Baert, R. Jonckheere, V.V. Moschalkov, and Y. Bruynseraede, Phys. Rev. B **53**, R2983 (1996)

[7] A.N. Grigorenko, G.D. Howells, S.J. Bending, J. Bekaert, M.J. Van Bael, L. Van Look, V.V. Moschalkov, Y. Bruynseraede, G. Borghs, I.I. Kaya, and R.A. Stradling, Phys. Rev. B **63**, 052504 (2001).

[8] S. Field *et al.*, cond-mat/0003415 (unpublished).

[9] J.I. Martín, M. Vélez, J. Nogués, and I.K. Schuller, Phys. Rev. Lett. **79**, 1929 (1997); D.J. Morgan and J.B. Ketterson, *ibid.* **80**, 3614 (1998); Y. Jaccard, J.I. Martín, M.-C. Cyrille, M. Vélez, J.L. Vicent, and I.K. Schuller, Phys. Rev. B **58**, 8232 (1998); A. Terentiev, D.B. Watkins, L.E. De Long, D.J. Morgan, and J.B. Ketterson, Physica C **324**, 1 (1999); A. Terentiev, D.B. Watkins, L.E. De Long, L.D. Cooley, D.J. Morgan, and J.B. Ketterson, Phys. Rev. B **61**, R9249 (2000).

[10] Y. Fasano, J.A. Herbsommer, F. de la Cruz, F. Pardo, P.L. Gammel, E. Bucher, and D.J. Bishop, Phys. Rev. B **60**, R15 047 (1999).

[11] J.I. Martín, M. Vélez, A. Hoffmann, I.K. Schuller, and J.L. Vicent, Phys. Rev. Lett. **83**, 1022 (1999); J.I. Martín, M. Vélez, A. Hoffmann, I.K. Schuller, and J.L. Vicent, Phys. Rev. B **62**, 9110 (2000).

[12] C. Reichhardt, C.J. Olson, and F. Nori, Phys. Rev. B **57**, 7937 (1998).

[13] D.R. Nelson and B.I. Halperin, Phys. Rev. B **19**, 2457 (1979).

[14] A. Chowdhury, B.J. Ackerson, and N.A. Clark, Phys. Rev. Lett. **55**, 833 (1985); J. Chakrabarti, H.R. Krishnamurthy, A.K. Sood, and S. Sengupta, *ibid.* **75**, 2232 (1995); Q.-H. Wei, C. Bechinger, D. Rudhardt, and P. Leiderer, *ibid.* **81**, 2606 (1998); C. Bechinger, M. Brunner, and P. Leiderer, *ibid.* **86**, 930 (2001).

[15] M. Franz and S. Teitel, Phys. Rev. Lett. **73**, 480 (1994); M. Franz and S. Teitel, Phys. Rev. B **51**, 6551 (1995).

[16] S. Hattel and J.M. Wheatley, Phys. Rev. B **51**, 11 951 (1995).

[17] E.R. Dufresne and D.G. Grier, Rev. Sci. Instrum. **69**, 1974 (1998).

[18] E.R. Dufresne, G.C. Spalding, M.T. Dearing, S.A. Sheets, and D.G. Grier, cond-mat/0008414 (unpublished).

[19] P. Korda, G. C. Spalding, and D. G. Grier, Bull. Am. Phys. Soc. (to be published).

[20] L. Radzihovsky, E. Frey, and D. R. Nelson, Phys. Rev. E **63**, 031503 (2001).

[21] V.I. Marconi and D. Domínguez, Phys. Rev. Lett. **82**, 4922 (1999); C. Reichhardt and G.T. Zimanyi, Phys. Rev. B **61**, 14 354 (2000); G. Carneiro, *ibid.* **62**, R14 661 (2000).

[22] L. Radzihovsky, Phys. Rev. Lett. **74**, 4923 (1995).

[23] M.R. Eskildsen, P.L. Gammel, B.P. Barber, U. Yaron, A.P. Ramirez, D.A. Huse, D.J. Bishop, C. Bolle, C.M. Lieber, S. Oxx, S. Sridhar, N.H. Andersen, K. Mortensen, and P.C. Canfield, Phys. Rev. Lett. **78**, 1968 (1997); M.R. Eskildsen, P.L. Gammel, B.P. Barber, A.P. Ramirez, D.J. Bishop, N.H. Andersen, K. Mortensen, C.A. Bolle, C.M. Lieber, and P.C. Canfield, *ibid.* **79**, 487 (1997); M.R. Eskildsen, A.B. Abrahamsen, D. López, P.L. Gammel, D.J. Bishop, N.H. Andersen, K. Mortensen, and P.C. Canfield, *ibid.* **86**, 320 (2001).

[24] D. McK Paul, C.V. Tomy, C.M. Aegerter, R. Cubitt, S.H. Lloyd,

E.M. Forgan, S.L. Lee, and M. Yethiraj, Phys. Rev. Lett. **80**, 1517 (1998).

[25] P.L. Gammel, D.J. Bishop, M.R. Eskildsen, K. Mortensen, N.H. Andersen, I.R. Fisher, K.O. Cheon, P.C. Canfield, and V.G. Kogan, Phys. Rev. Lett. **82**, 4082 (1999).

[26] V.G. Kogan, A. Gurevich, J.H. Cho, D.C. Johnston, M. Xu, J.R. Thompson, and A. Martynovich, Phys. Rev. B **54**, 12 386

(1996); V.G. Kogan, P. Mikranovic, L.J. Dobrosavljevic-Grujic, W.E. Pickett, and D.K. Christen, Phys. Rev. Lett. **79**, 741 (1997).

[27] A. Brass and H.J. Jensen, Phys. Rev. B **39**, 9587 (1989).

[28] H.J. Jensen, A. Brass, A.C. Shi, and A.J. Berlinsky, Phys. Rev. B **41**, 6394 (1990).